A GEOMETRICAL MODEL OF SOIL BIDIRECTIONAL REFLECTANCE IN THE VISIBLE AND NEAR-INFRARED RANGE

J. CIERNIEWSKI
Adam Mickiewicz University, Institute of Physical Geography, Fredry 1, 61-701 Poznań (Poland)

M. VERBRUGGHE
I.N.R.A. Bioclimatologie, B.P. 91, 84143 Montfavet Cedex (France)

ABSTRACT:

A model dealing with the influence of soil surface roughness, solar illumination and the viewing of soil surface on soil reflectance in the visible and reflective near-infrared range along the solar principal plane is discussed. The model is based on the assumption that the reflectance from anisotropic rough soil surfaces is strongly correlated with the area of sunlit soil surface being essentialy reduced by the area of shaded soil fragments. Wave energy leaving the sunlit soil fragments is directly proportional to the energy coming to them, i.e., it depends on the incidence angle of the sunbeams directly illuminating these fragments. Spheroids, characterized by their horizontal and vertical radii, lying on an horizontal surface at a given distance, simulate the soil surface. The model was tested using soil bidirectional reflectance data acquired on a bare field of an alluvial plain covered by regularly spread pebbles. The spectral data were measured by a three-channel field radiometer CIMEL simulating the SPOT (HRV) bands. The regression analysis was performed separately for the three channels using 169 pairs of data for 15 solar zenith angles (SZA) varied from 25° to 66°. The relative reflectance factor may be predicted with a mean deviation from the measured reflectance data lower than 0.09 for the SZA lower than 50° and lower than 0.14 for the SZA higher than 50°.

KEY WORDS: Geometrical model, Bidirectional soil reflectance, Visible and Near-infrared range

1. INTRODUCTION

Remotely sensed data on soil surfaces like vegetation canopies have non-Lambertian reflectance properties. Rough soil surfaces usually display variations in brightness due to the direction of irradiation and also the direction along which reflection is observed. A soil surface seems to be the brightest from the direction which give the lowest proportion of shaded fragments. The scattering properties of bare soil, showing a backscatter reflectance peak towards the position of the sun, are displayed by field reflectance measurements of bare soils taken by Kimes and Sellers (1985). Milton and Webb (1987) present the results of ground measurements of ploughed bare soils, clearly indicating the angular asymmetry of reflectance around the nadir. The reflectance of the soils increases with the increase in the view zenith angle if the sensor was directed towards the solar beam. The peak of backscatter radiation become less pronounced at a low solar zenith angle. Deering et al. (1990) have supplied evidence that soil reflectance could clearly have both a backscatter and a forwardscatter character. They demonstrated it on an example of bidirectional reflectance data of an alkali flat bare soil and a dune sand flat surface with uniform ripples and composed of nearly pure gypsum crystals.

Soil reflectance generated by most of the existing models characterizing minimum shadowing from anti-solar directions has shown a strong backscattering regime. Otterman and Weiss's model (1984) treats soils as a field of randomly located thin vertical cylinders, illuminated by a direct solar beam. The model of Norman et al. (1985) was developed on the assumption that the shadowing of larger soil particles or aggregates, simulated by cuboids, had a stronger influence on the soil reflectance distribution than scattering properties of bare soil particles of silt and clay. The smaller the shadowing, the higher the reflectance of the modeled surface. The Monte Carlo reflectance model of soil surfaces, created by Cooper and Smith (1985), assumes that the soil is a perfect diffuse scatterer at a microscopic level. The probability that a photon will be scattered at a given angle depends only on the orientation of the micro soil surface. Hapke's model, used by Pinty et al. (1989) for modeling soil reflectance, describes a soil surface as a substrate composed of particles which multiply scatter solar radiation of an isotropic character. Simple soil surface roughness parameters are replaced here by five others connected with the physical principles of reflectance. Jacquemoud et al. (1992), using the radiative transfer model based on the same model of Hapke, found that the single scattering albedo is only dependent on wavelength. The roughness parameter belongs to wavelength-independent parameters. The model of Irons et al. (1992) describes soil surfaces as uniform opaque spheres regularly spaced on a horizontal

surface. Both, direct and isotropically diffuse solar radiation in shadow illuminate the simulated soil surface. The model assumes that reflectance from any point on a sphere as well as on the horizontal surface is Lambertian. The models mentioned above was validated by ground measurements of soil reflectance demonstrating a close similarity to the model-generated data.

Relations found between remotely sensed data and parameters of the illumination and viewing geometry of interpreted surfaces have been used to correct their images before classification. The dependence of the data upon the sensor view angle is especially important for airborne and satellite scanners viewing the surfaces at wide scan angles (Barnsley, 1984; Foody, 1988; Kowalik et al., 1982; Royer at al., 1985). The directional reflectance of soil surfaces as non-Lambertian reflectors has been explained by interactions of the directional component of solar irradiation with irregularities of the surfaces, i.e., soil aggregates, clods and soil microrelief configurations. These rough elements produce shadowing effects which change the level and angular distribution of solar energy leaving the soil surfaces (Cierniewski, 1987; Cooper and Smith, 1985; Graetz and Gentle, 1982; Huete, 1987; Milton and Webb, 1987; Norman et al., 1985; Pech et al., 1986).

The aim of this paper is to present a mathematical model of the influence of soil surface roughness, solar illumination and viewing of a soil surface on soil reflectance in the visible and reflective near-infrared range. It is a further improvement of the previous model (Cierniewski, 1989) and the derived version of the model developed by Verbrugghe and Cierniewski (1993).

2. METHODS

2.1. The model

The model assumes that wave energy in the visible and near-infrared range reflected from anisotropic soil surfaces is strongly correlated with the area of sunlit soil surface fragments and significantly reduced by the area of shaded soil fragments. Furthermore, the energy leaving the sunlit soil fragments is directly proportional to the energy coming to them, that is, it also depends on the angle of incidence of the sunbeams on these directly illuminated parts.

The model predicts the reflectance distribution of an horizontal soil surface along the solar principal plane in the wavelength range mentioned above. Equal-sized spheroids of horizontal (a) and vertical (b) radii, lying on a horizontal plane simulate the soil surface (Fig. 1). They are arranged on the horizontal surface so their centers in the horizontal projection are at the distance d, independently of the azimuthal position of the solar principal plane. This regularity in the spacing of the spheroids expresses isotropic features of the simulated soil surface geometry. The shadowed and sunlit fragments of the structure are observed by a sensor inside of the (r_f) and the (r_b) radii of the basic view area of the sensor which changes with the view zenith angle (θv) as:

$$r_f = r_b = 1/2\ d \cos\theta v. \tag{1}$$

Along these radii the model calculates segments of the sunlit (I) and shadowed fragments (S) of the given spheroid (Is, Ss), the adjoining spheroid (Ia, Sa), and the ground surface between the spheroids (Ig, Sg). The model divides curvilinear slopes of the calculated sunlit soil surface segments into many (j) simple linear sub-slopes of the angle βi. The position of border points between the sunlit and shadowed fragments, and also the sub-slope angles were found analytically by solving trigonometrical equations. The βi angles in relation to the azimuth position of the soil slopes (ϕr), and angles of the sunbeam direction, θs and ϕs, decide about wave energy reaching these sunlit fragments. This energy is determined using the factor $E_{\beta i}$ as:

$$E_{\beta i} = \cos\theta s \cos\beta i + \sin\beta i \sin\theta s\ (\sin\phi s \sin\phi r + \cos\phi s \cos\phi r), \tag{2}$$

where ϕr is 90° for the forward βi angles and 270° for the backward βi; ϕs equals 90° for all the solar azimuth angles. The factor $E_{\beta i}$ is 1 if the sunbeams reach the analyzed slope perpendicularly. It equals 0 when the sunbeams are tangential to a given slope. Negative values of this factor mean that the sunbeams do not reach the slope directly, i.e., that it slope is shaded.

Assuming that the total energy leaving the sunlit soil fragments is directly proportional to $E_{\beta i}$ and the length of sunlit soil sub-segments li, and that the energy leaving the shaded fragments of an isotropic distribution is proportional to the length of shaded segments, relative luminance of the analyzed soil surface (L) visible to the sensor from the given direction (θv) can be formulated as:

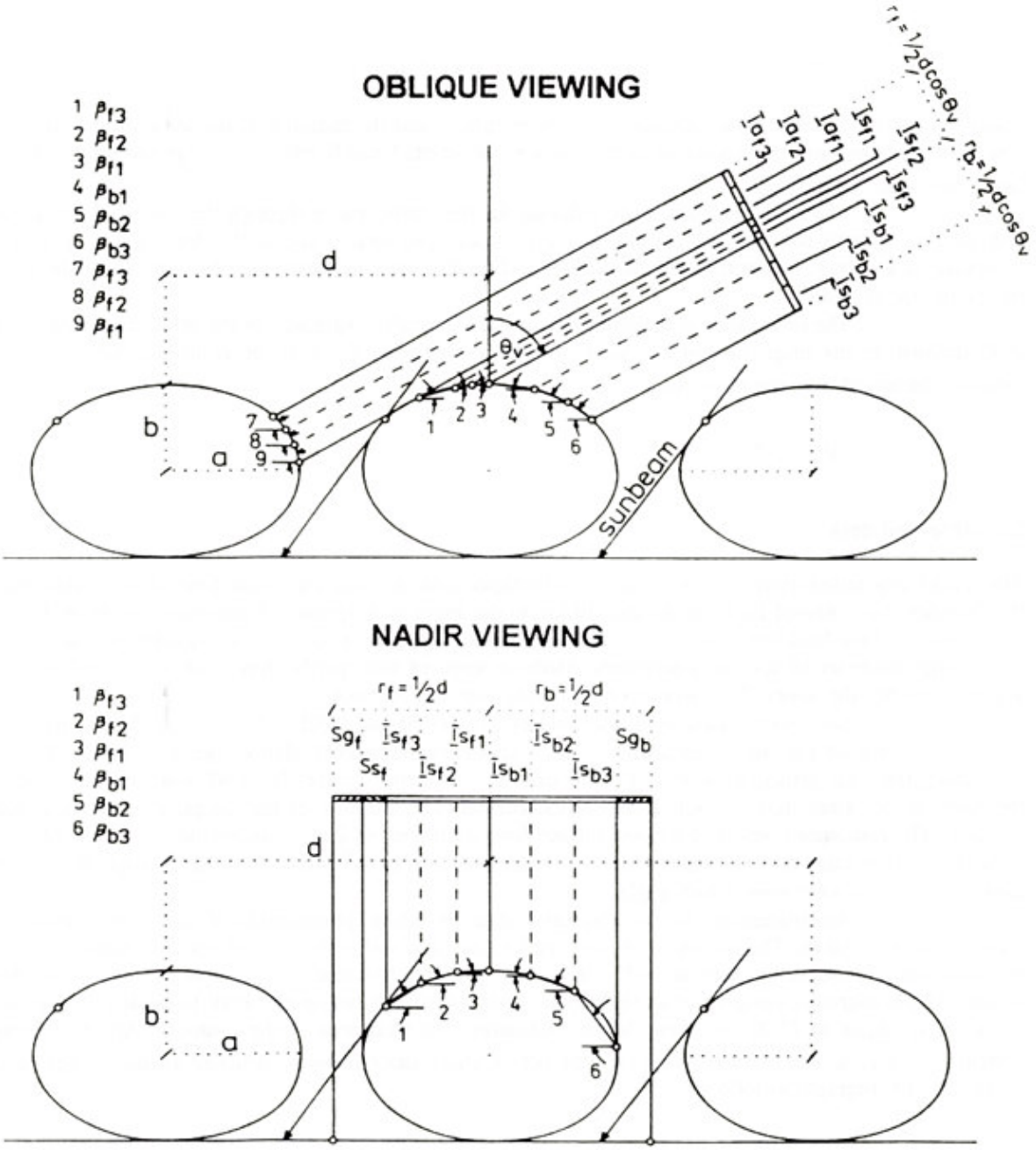

Figure 1. Geometry of the illuminated soil surface along the solar principal plane with sunlit (I) and shaded (S) sub-segments of the given spheroid (Is, Ss), the adjoining spheroids (Ia, Sa) and the ground between the spheroids (Ig, Sg), situated at angles βi. Symbols r_f and r_b describe the radii of the basic view distance.

$$L = SE/SS; \tag{3}$$

$$SE = \sum_{i=1}^{j} (Es_{\beta fi}\, Is_{fi})\,(1-f) + Ss_f\, f + \sum_{i=1}^{j} (Es_{\beta bi}\, Is_{bi})\,(1-f) + Ss_b\, f + \sum_{i=1}^{j} (Ea_{\beta fi}\, Ia_{fi})\,(1-f) + S_{af}\, f +$$

$$\sum_{i=1}^{j} (Ea_{\beta bi}\, Ia_{bi})\,(1-f) + Sa_b\, f + Eg_f\, Ig_f\,(1-f) + Sg_f\, f + Eg_b\, Ig_b\,(1-f) + Sg_b\, f$$

$$SS = Is_f + Ss_f + Is_b + Ss_b + Ia_f + Sa_f + Ia_b + Sa_b + Ig_f + Sg_f + Ig_b + Sg_b,$$

where f is the ratio between the radiance of a shaded surface and the radiance of the same illuminated surface when the sunbeams are perpendicular to the surface; subscripts f and b refer to the (r_f) and (r_b) radii of the basic view area, respectively.

The model calculates the radiance for the profile going through the center of the spheroids, and then for several next profiles parallel to the first one. The total radiance (Lt) for a given view angle is computed as a average values from all the profiles and the flat space between the spheroids, where the L for the flat plane equals cosθs.

The reflectance of the simulated surface is finally expressed by the relative reflectance factor (FR) defined as the proportion of the total luminance measured from an off-nadir direction (Lt_o) to the radiance measured from the nadir (Lt_n):

$$FR = Lt_o/Lt_n\,. \tag{4}$$

2.2. Observed data

The model was tested using soil bidirectional reflectance data acquired on a bare field of an alluvial plain of the Durance river, named La Crau, located 40 km to the south of Avignon, 25 km south-east from Arles, and 15 km north of the Mediterranean Sea in southern France. The plain is covered by regularly spread pebbles of an average diameter of several centimeters. Medium textured soil, partly overgrown by natural vegetation, appears between the stones. This area serves as winter pastures for sheep.

Soil spectral data were measured by a three-channel (SX1: 0.50-0.59 μm, SX2: 0.61-0.68 μm and SX3: 0.79-0.89 μm) field radiometer CIMEL simulating the SPOT (HRV) bands. It collected radiance data along the solar principal plane in 13 directions at view zenith angles from 60° towards the sun through the nadir to 60° away from the sun at 10° of increments. The duration of the complete sequence is about 4 minutes. The radiometer observed the soil surface from a distance of 2 m. This instrument with a 12° field of view (FOV) integrated reflected energy from a circular area of 0.14 m^2 at a 0° view zenith angle to an elliptical area of 0.29 m^2 at a 60° view zenith angle.

Simultaneously to the radiometric data collecting, photographs of the target, viewed by the radiometer, were taken. The photographs were used to measure soil surface roughness parameters. They were obtained using photographs taken at the 0° view zenith angle for five selected values of the solar zenith angles. In the five photographs, contours of all the pebbles lying within the radiometer FOV (a circle on the ground of a radius (r_n) equal to 21.02 cm) were drown. Measuring the total area of the contours (Ap) by a computer system for image analysis named VISILOG, the pebble area index (AI) was calculated as the average value for all the five photographs as follows:

$$AI = Ap/(\pi\, r_n^2) \tag{5}$$

Then, the average relative distance between the pebbles divided by their average radius (d/a) was computed as:

$$d/a = \sqrt{\pi/AI}\,. \tag{6}$$

The parameter describing the shape of the pebbles, i.e., the average proportion between their vertical and horizontal radii (b/a), was determined after finishing the reflectance data collection. The b and a sizes of each of the pebbles lying within the radiometer nadir FOV was measured directly by a ruler.

A linear regression analysis of soil reflectance data measured by the CIMEL radiometer and predicted by the model was used here. The reflectance data corresponding with positions of the radiometer for which the instrument cast a shadow on the observed soil surface, were eliminated from the analysis.

3. RESULTS

The accuracy of the soil reflectance distribution in the view zenith angle function generated by the model was tested on an untypical soil surface. The surface created by pebbles makes easier a geometrical description of the soil surface for reflectance modeling. The average proportion between the vertical (b) and the horizontal radii (a) of the pebbles was 0.56. The average pebble area index (AI) measured from the photographs within the radiometer field-of-view (FOV) at the nadir was 0.56, and the average relative distance between the pebbles (d/a) was 2.37. The ratio (f) was evaluated by substituting different values to the model and looking for the values which gives the highest correlation coefficient and the lowest root mean square between the model-generated and observed soil reflectance data. The value of the f equals 0.20 was found in the way for all the three channels.

The regression analysis was performed separately for the three channels, using 169 pairs of data representing the soil surface under different illumination conditions. The analysis yielded the highest coefficient of determination $r^2 = 0.94$ for the SX2 channel and the lowest one, $r^2 = 0.88$ for the SX3 channel (Fig. 2). The relative reflectance factor may be predicted for the channels SX1 and SX3 with a mean deviation (rms) from the measured reflectance data of about 0.07 - 0.08, and 0.06 for the channel SX2.

The coefficient of determination and the root mean square (rms) computed separately for 15 solar positions for the three channels are presented in Table 1. For all these three channels the measured reflectance curves generally show a similar fit to those predicted by the model when the solar zenith angles are lower than 50° (Fig. 3). The precision of the fit is between 89% and 97%. For higher solar zenith angles (SZA) than 50° the precision for the SX1 and the SX3 dicreases to 82%. The best correlation demonstrate the data for the channel SX2 for which the coefficient of determination does not reach the lower value than 93%, even for higher SZA than 50°. The relative rms difference between the generated and measured reflectance factor for SZAs lower than 50° was less than 0.06 - 0.09 for all the channels. When solar zenith angles were higher than 50° the root mean square for them reached values lower than 0.14.

Table 1. Coefficient of determination (r^2) and root mean square (rms) for measured and predicted reflectance data for different illlumination conditions defined by the solar zenith angle (SZA) and the solar azimuth angle (SAA). N is the number of the data included in the analysis.

			SX1		SX2		SX3	
SZA	SAA	N	r^2	rms	r^2	rms	r^2	rms
25.2	174.0	11	0.92	0.07	0.97	0.04	0.93	0.06
25.5	192.4	11	0.94	0.06	0.98	0.03	0.96	0.04
27.7	150.1	12	0.93	0.07	0.96	0.05	0.96	0.06
28.8	214.8	11	0.96	0.05	0.98	0.05	0.96	0.05
31.6	135.2	11	0.89	0.09	0.95	0.06	0.91	0.07
33.7	230.5	12	0.94	0.06	0.97	0.04	0.96	0.05
36.5	123.2	12	0.93	0.09	0.96	0.08	0.91	0.09
40.3	243.5	11	0.97	0.05	0.98	0.04	0.97	0.05
41.3	114.8	11	0.91	0.09	0.93	0.08	0.89	0.09
46.8	253.0	11	0.95	0.07	0.97	0.05	0.95	0.06
48.3	105.2	11	0.95	0.05	0.95	0.06	0.89	0.09
54.1	98.5	11	0.93	0.07	0.94	0.08	0.82	0.10
57.3	264.8	11	0.90	0.07	0.95	0.06	0.88	0.08
62.5	90.2	12	0.91	0.08	0.94	0.09	0.85	0.12
66.0	266.8	12	0.84	0.14	0.93	0.11	0.83	0.14

The largest incompatibility of the measured data with the predicted ones refers to the forwardscattering range of the relative reflectance factor. It is caused by a fact that specular features of the soil reflection are disregarded in the modelling.

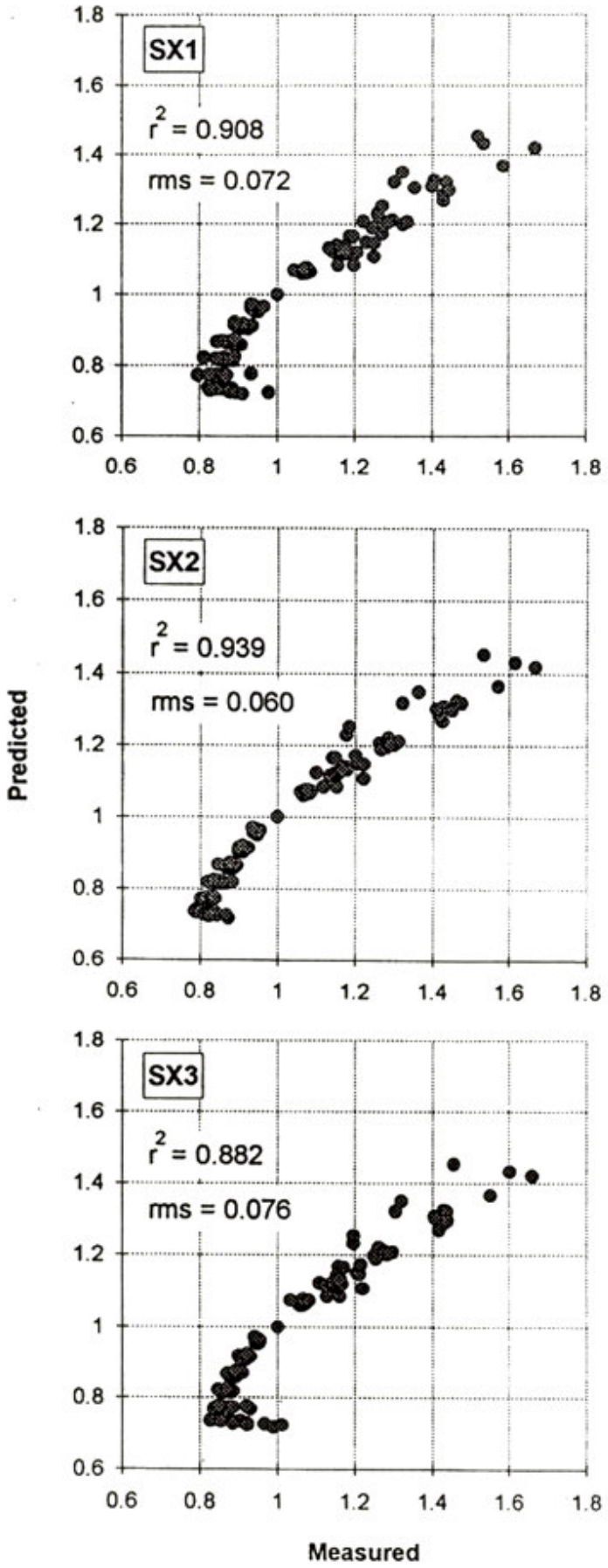

Figure 2. Relationship between measured and predicted soil reflectance factors for wavelengths corresponding to the three (SX1, SX2 and SX3) channels of the CIMEL radiometer.

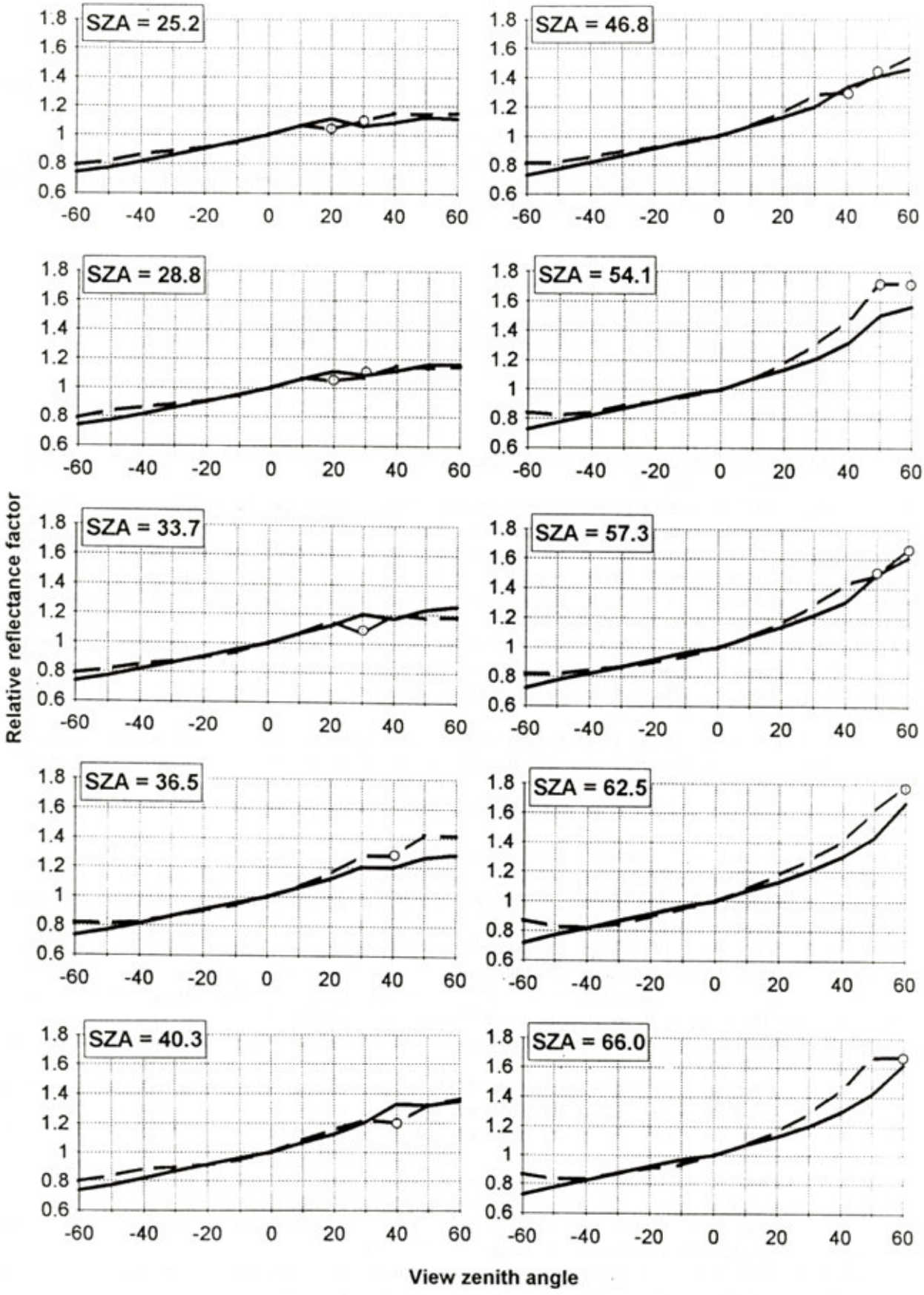

Figure 3. Relationship between the reflectance factor along the solar principal plane for the channel SX2 predicted by the model (solid line) and that measured (dashed line) for selected solar zenith angles (SZA). Symbol o - data colleted in conditions when the radiometer casts a shadow on the observed surface.

4. CONCLUSIONS

The geometrical model of soil bidirectional reflectance presented in this paper demonstrates a clear backscattering character of the reflectance distribution along the solar principal plane.

The model-generated bidirectional reflectance seem to find corroboration in the results of the correlation analysis carried out. Howewer, an examination of the accuracy of the model against more typical soils and a larger sample of measured reflectance data would be very interesting, especially in experiments in which the soil roughness state could be controlled adequately.

5. AKNOWLEDGMENTS

The authors wish to thank Jean Francois Hanocq (Bioclimatologie, Montfavet) for his help in measurements. This work was partly supported by a grant from the French Ministry of Research and Technology.

6. REFERENCES

Barnsley, M. J., 1984. Effects of off-nadir view angles on the detected spectral response of vegetation canopies. Int. J. Remote Sens., 15: 715-728.

Cierniewski, J., 1987. A model for soil surface roughness influence on the spectral response of bare soils in the visible and near-infrared range. Remote Sens. Environ., 123: 97-115.

Cierniewski, J., 1989. The influence of the viewing geometry of bare rough soil surfaces on their spectral response in the visible and near-infrared range. Remote Sens. Environ., 127: 135-142.

Cooper, K. D. and Smith J. A., 1985. A Monte Carlo reflectance model for soil surfaces with three-dimensional structure. IEEE Trans. Geosci Remote Sens., 1GE-23: 668-673.

Deering, D. W., Eack, T. F., and Otterman, J., 1990. Bidirectional reflectances of selected desert surfaces and their three-parameter soil characterization. Agricultural and Forest Meteorology 1, 52: 71-93.

Foody, G. M., 1988. The effects of viewing geometry on image classification. Int. J. Remote Sens., 19: 1909-1915.

Graetz, R. D. and Gentle, M. R., 1982. A study of the relationship between reflectance characteristics in the Landsat wavebands and the composition and structure of an Australian semi-arid rangeland. Photogramm. Eng. Remote Sens., 148: 1721-1736.

Huete, A. R., 1987. Soil and Sun angle interactions on partial canopy spectra. Int. J. Remote Sens., 18: 1307-1317.

Irons, J. R., Campbell, G. S., Norman, J. M., Graham, D., W., and Kovalick, W. M., 1992. Prediction and measurement of soil bidirectional reflectance. IEEE Trans. Geosci Remote Sens., 30, 2: 249-260.

Jacquemoud, S., Baret, F., and Hanocq, J. F., 1992. Modeling spectral and bidirectional soil reflectance. Remote Sens. Environ., 41:123-132.

Kimes, D. S., Seller, P. J., 1985. Inferring hemispherical reflectance of the Earth's surface for global energy budget from remotely sensed nadir or directional radiance values. Remote Sens. Environ., 118: 205-223.

Kowalik, S., Marsh, S. E., and Lyon, R. J. (1982), A relation between Landsat digital numbers, surface reflectance, and the cosine of the solar zenith angle. Remote Sens. Environ., 112: 39-55.

Milton, E., J. and Webb, J., P., 1987. Ground radiometry and airborne, multispectral survey of bare soils. Int. J. Remote Sens., 18: 3-14.

Norman, J. M., Welles, J. M. and Walter, E. A., 1985. Contrast among bidirectional reflectance of leaves, canopies, and soils. IEEE Trans. Geosci. Remote Sens., 1GE-23: 659-667.

Otterman, J., Weiss, G. H., 1984. Reflectance from a field of randomly located vertical protrusions. Appl. Opt., 123: 1931-1936.

Pech, R. P., Graetz, R. R., Davis, A. W., 1986. Reflectance modelling and the derivation of vegetation indices for an Australian semi-arid shrubland. Int. J. Remote Sens., 17: 389-403.

Pinty, B., Verstraete, M. M., and Dickinson, R. E., 1989. A physical model for predicting bidirectional reflectances over bare soils. Remote Sens. Environ., 127: 273-288.

Ranson, K. J., Biehl, L. L., and Bauer, M. E., 1985. Variation in spectral response of soybeans with respect to illumination, view and canopy geometry. Int. J. Remote Sens., 16: 1827-1842.

Royer, A., Pierre, V., and Bonn, F., 1985. Evaluation and correction of viewing angle effects on satellite measurements of bidirectional reflectance. Photogramm. Eng. Remote Sens., 151: 1899-1914.

Verbrugghe, M. and Cierniewski, J., 1993. Effects of sun and view geometries on cotton bidirectional reflectance. Test of a geometrical model. Submitted to Remote Sens. Environ. Special Issue.